Acoustic driven flow and lattice Boltzmann simulations to study cell adhesion in biofunctionalized µ-fluidic channels with complex geometry

Mohammad A. Fallah, V. M. Myles, T. Krüger, Kumudesh Sritharan, Achim Wixforth, F. Varnik, S. W. Schneider, Matthias F. Schneider

Acoustic driven flow and lattice Boltzmann simulations to study cell adhesion in biofunctionalized μ-fluidic channels with complex geometry

M. A. Fallah, V. M. Myles, T. Krüger, et al.

View Online   **Export Citation**

ARTICLES YOU MAY BE INTERESTED IN

Acoustic driven flow and lattice Boltzmann simulations to study cell adhesion in biofunctionalized μ-fluidic channels with complex geometry

M. A. Fallah,[1,a)] V. M. Myles,[1,a)] T. Krüger,[2] K. Sritharan,[1] A. Wixforth,[1] F. Varnik,[2] S. W. Schneider,[3,b)] and M. F. Schneider[4,b)]

[1]*Department of Experimental Physics I, University of Augsburg, Augsburg 86159, Germany*
[2]*Microstructure Physics and Metal Forming, Max-Planck-Institut für Eisenforschung (MPIE), Düsseldorf 40237, Germany*
[3]*Department of Dermatology, Venereology and Allergology, Experimental Dermatology, Medical Faculty Mannheim, Heidelberg Ruprecht-Karls-University, 68163 Mannheim, Germany*
[4]*Department of Mechanical Engineering, Boston University, Boston, Massachusetts 02215, USA*

Accurately mimicking the complexity of microvascular systems calls for a technology which can accommodate particularly small sample volumes while retaining a large degree of freedom in channel geometry and keeping the price considerably low to allow for high throughput experiments. Here, we demonstrate that the use of surface acoustic wave driven microfluidics systems successfully allows the study of the interrelation between melanoma cell adhesion, the matrix protein collagen type I, the blood clotting factor von Willebrand factor (vWF), and microfluidic channel geometry. The versatility of the tool presented enables us to examine cell adhesion under flow in straight and bifurcated microfluidic channels in the presence of different protein coatings. We show that the addition of vWF tremendously increases (up to tenfold) the adhesion of melanoma cells even under fairly low shear flow conditions. This effect is altered in the presence of bifurcated channels demonstrating the importance of an elaborate hydrodynamic analysis to differentiate between physical and biological effects. Therefore, computer simulations have been performed along with the experiments to reveal the entire flow profile in the channel. We conclude that a combination of theory and experiment will lead to a consistent explanation of cell adhesion, and will optimize the potential of microfluidic experiments to further unravel the relation between blood clotting factors, cell adhesion molecules, cancer cell spreading, and the hydrodynamic conditions in our microcirculatory system. © *2010 American Institute of Physics.*
[doi:10.1063/1.3396449]

I. INTRODUCTION

The increasing evidence that cancer cell spreading is accompanied by an activation of the coagulatory machinery and therefore may result in thrombotic events calls for thorough examination of tumor cells under defined shear flow conditions.[1–5] Among different coagulatory proteins von Willebrand factor (vWF) plays a key role in initiating the cellular hemostasis by binding platelets even under high shear flow conditions.[2] vWF is stored in Weibel–Palade bodies in

---

[a)]These authors contributed equally to this work.
[b)]Authors to whom correspondence should be addressed. Electronic addresses: mfs@bu.edu and stefan.schneider@medma.uni-heidelberg.de.

4, 024106-1

endothelial cells and in platelets. Upon endothelial cell activation, followed by an intracellular calcium or cAMP increase, Weibel–Palade bodies fuse with the endothelial cell membrane to release vWF. After vWF release, the protein is stored in the subendothelium matrix or delivered in the blood stream.[6,7] Under high shear flow conditions the protein exhibits a globule-stretched transition which leads to an extensive exposure of binding sites to the surrounding blood supporting platelet binding.[8] While the relation between vWF and blood platelet immobilization is well described,[9] vWF and its interactions with melanoma cells under flow conditions remain almost entirely unclear. Here, we present a novel microfluidic tool, which allows for the study of the complex interplay between protein enhanced cell adhesion and complex microfluidic channel geometry. Surface acoustic wave (SAW) driven microfluidics are used to examine the regime of low Reynolds numbers (Re), characterizing the flow conditions of our human vascular system. Indeed, generating flow at low Re conditions has been demonstrated to be a challenging task and many innovative microfluidic solutions for cellomics and proteomics, known as micrototal analysis systems (μTAS), have been designed to overcome these problems. The fluids in such systems are usually driven by external means such as pneumatic pressure or syringe pumps. Handling obstacles and the possibility of contamination are common drawbacks of such systems.[10] Even internal pumping methods like electro-osmotic flow or valve-type micropumps which operate based on piezoelectric actuations exhibit some deficiencies which are detailed elsewhere.[11,12]

Driven by the requirements mentioned, we have developed a novel method for pumping fluids at low Re. The method meets the expectations for flexible design which can be used to mimic various two- and three-dimensional geometries encountered in our microcirculatory system, and can handle extremely small volumes of liquid (μl-pl). The technique, which has been successfully employed in multiple research areas within our laboratories,[13–16] is based on the interaction of SAWs with a liquid at the surface at which the waves propagate. The planar arrangement not only allows for controlled microfluidic flow ($\sim$10 μl) in complex geometries, such as bifurcations and stenotic conditions, but enormously facilitates surface biofunctionalization with proteins or even confluent cell layers in these small volumes. The hydrodynamic conditions are characterized by combining experimental measurements of the flow field using tracer beads with lattice Boltzmann computer simulations. The latter allows us to calculate the equivalent wall shear rate necessary when estimating the forces acting during cell adhesion. Finally, the biocompatible system is relatively low priced, easy to handle, and can be mounted on any typical standard microscope. Here, we demonstrate that this technique is suitable to study the interrelation between blood clotting, hemodynamic flow conditions, and caner cell adhesion in simple, straight, as well as bifurcated microfluidic channels and reveals a strong increase in adhesion in the presence of vWF.

II. MATERIALS AND METHODS

A. The acoustic nanopump

The general design of our microfluidic flow chamber on a chip is depicted in Figs. 1(a) and 1(b). The heart of the channel, the nanopump, is based on acoustically driven flow (Fig. 1) in which SAW technology is applied to create surface acoustic streaming.[17–23] In brief, a SAW is essentially a sound wave of about 1 nm amplitude and wavelength of typically a few micrometers traveling along a solid-air interface. Due to the poor impedance coupling between substrate and air (large difference in sound velocities in the mediums), only very little energy is dissipated for this "pure mode." However, when a SAW encounters a solid-liquid interface, the impedance coupling changes drastically, causing a large dissipation of acoustic energy into the fluid. The energy dissipation causes an exponential decay of the SAW amplitude within a characteristic length scale of a few wavelengths, which in turn causes an acoustic pressure gradient driving the liquid to flow; an effect called acoustic streaming [Fig. 1(a)]. Considering a typical channel length of a couple of centimeters and a decay length of $\sim$100 μm, the pump essentially acts as a pointlike pressure source driving the liquid to flow according to conservation of mass.

Here, the SAW is generated on an anisotropic piezoelectric material (LiNbO$_3$, 128° y-cut, z propagating) in order to excite the Rayleigh mode, the most pronounced surface wave. A pair of
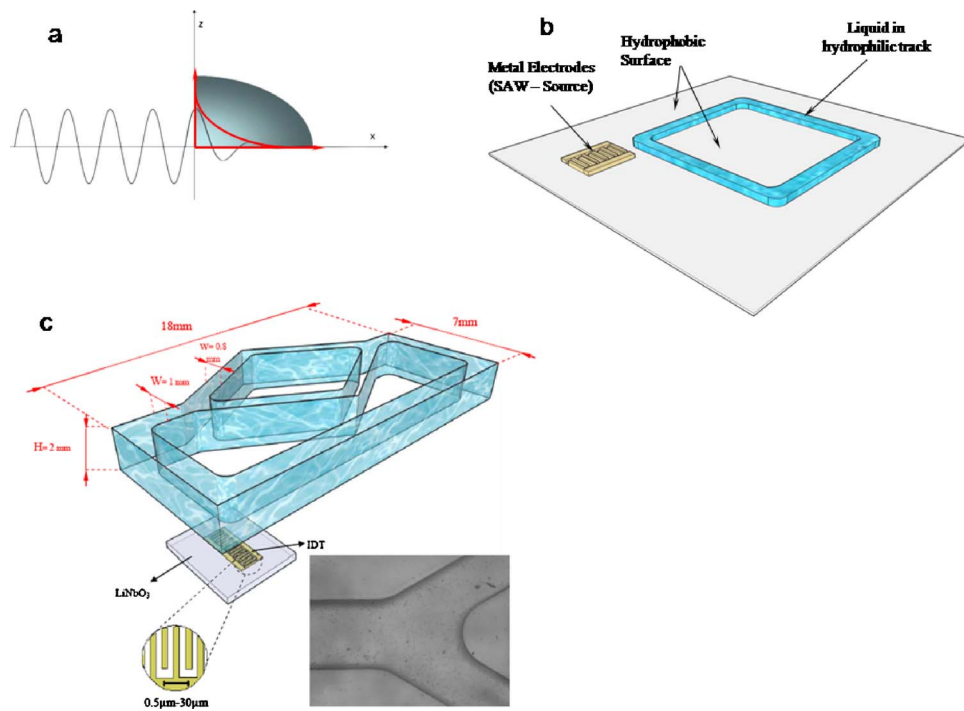
FIG. 1. (a) Schematic representation of the surface acoustic streaming. The SAW is generated on a piezoelectric material (LiNbO$_3$) employing IDTs and propagates on the solid-air interface. When the wave reaches the solid-liquid interface, acoustic energy is transmitted into the fluid, creating a pressure gradient (shown in red). This pressure gradient drives a continuous flow along the channel. (b) Planar chip with a two-dimensional track containing straight channels. The race track shaped channel consists of a planar hydrophilic track on an otherwise hydrophobic piezoelectric substrate (LiNbO$_3$). A SAW propagates from the IDT (seen on the right) into the direction of the microfluidic channel and causes a localized pressure gradient at the point of entry into the liquid. This causes a homogeneous laminar flow throughout the channel (scale bar=4 mm). (c) Sketch of the bifurcated channel geometry. An IDT is placed to the lower left corner of the bifurcated channel. The IDT is fabricated by the deposition of gold electrodes on the piezoelectric substrate (LiNbO$_3$) and is operated at $f=164$ MHz. In order to avoid uncontrolled reflections of the SAWs, only $\frac{1}{2}$ of the chip is integrated inside the channels.

interdigitated metal electrodes is deposited on top of the substrate using standard lithography and fed with a high frequency voltage to generate the SAW. Each individual electrode consists of a set of interdigitated fingers [interdigitated transducers (IDTs)]. Due to the high sound velocity (c_{SAW}) of the SAWs ($\sim$4000 m/s) and a typical finger distance (λ) of 10 μm, the matching condition

$$f = c_{SAW}/\lambda \tag{1}$$

requires an input signal of high frequency ($\sim$100 Mhz−1 GHz), which is generated using a signal generator (voltage controlled oscillator "ZX95-200-S," Mini Circuits, USA, Brooklyn). To enable standard protocols for further surface functionalization, the entire surface, including the IDTs, is covered by 50 nm SiO$_x$ using standard sputtering methods. We have shown that this additional layer does not significantly affect the capability of acoustic streaming.[16] Due to the optical transparency of the piezoelectric material employed, we are able to mount the microfluidic chip onto an inverted microscope (Zeiss Axiovert 200, Zeiss, Göttingen, Germany) to study the dynamics of protein stretching and recoiling under different shear conditions.[8]

B. Design of the microfluidic channels

The geometrical structure of the channel is sketched using AUTOCAD software. The pattern can be transferred to a mold by photolithography or milling techniques. In the present case, the latter technique is applied. The mold has the negative pattern of the microchannel and is filled with

polydimethylsiloxane (PDMS) (Dow Corning GmbH, Wiesbaden, Germany), a biocompatible transparent polymer, to obtain the desirable channel structure. The channels produced by this method can be either opened or closed. Here, the closed channels design has been chosen to facilitate the application of computer simulations. The PDMS channel is sealed to the glass slide, which in turn is coupled directly to the chip. The use of a separate glass slide easily enables us to perform cell culture directly on the bottom of the microfluidic channel. The investigated channel geometries are shown in Figs. 1(b) and 1(c). They include both a straight channel, in the form of a rectangular track with rounded edges, and a channel with a bifurcation.

Bifurcated geometries are very common in our microcirculatory system; nevertheless, their abundance is not the only reason of their investigation. Combining acoustic streaming with bifurcated structures gives us the possibility to benefit from different fluid velocities in a single microchannel and a single experiment. By changing the cross section of the channel before and after bifurcation one can screen for the impact of different flow velocities on the adhesion of cells. The channel footprint and volume are $A \approx 56$ mm^2 and $V \approx 112$ mm^3, respectively.

C. Theoretical study of the hydrodynamics by lattice Boltzmann method

Different velocities imply different shear rates at the boundaries, which are calculated by feeding the computer simulation with experimental data. The hydrodynamic flow profile and the equivalent shear stress of the fluid in the bifurcation

$$\sigma_{eq} = \sqrt{\frac{1}{2}\sum_{\alpha\beta} \sigma_{\alpha\beta}\sigma_{\alpha\beta}} \tag{2}$$

can be numerically computed in lattice Boltzmann computer simulations. It is noteworthy to mention that shear rate (or shear stress) tensor is a full 3×3 tensor, but in the literature, shear rates are usually reported as scalars, the expected one for the simple shear flow.[24] For this reason, we have to compute a representative scalar from the tensor. The trace is not useful since it is zero for an incompressible fluid. The common approach is to compute the von Mises stress (magnitude) of the tensor, as defined in Eq. (2). This choice ensures that the effective shear rate extracted from the tensor is exactly the expected one for simple shear flow. The effective shear rate is the shear stress divided by the dynamic viscosity of the fluid,

$$\dot{\gamma}_{eq} = \sigma_{eq}/\mu. \tag{3}$$

In order to numerically compute the solution of the flow in the bifurcated channel, we use the lattice Boltzmann method (LBM). It is a relatively new but well understood approach to solve the full Navier–Stokes equation in the presence of even complex geometries.[25–30] Due to its robustness, simple coding, and parallelizability, the method enjoys steadily increasing attention. Especially in the recent years, many researchers have used LBM to simulate blood flow in the arterial and venous system.[31–34]

We have set up simulations with boundary conditions corresponding to the described bifurcation geometry. The only free simulation parameter apart from the fluid density and viscosity is the central inlet velocity. A value of $v = 1.4$ mm/s was measured in our experiments. The total volume flux through the channel is found to be slightly larger than $\phi = 1.4$ mm^3/s. A computational grid of $400 \times 286 \times 102$ lattice nodes has been used for the simulations. The visualizations of the flow profiles have been created using PARAVIEW.[35]

D. Biofunctionalization of the microchannels

1. Biofunctionalization with collagen

Biofunctionalization for different μ-fluidic patterns is usually a complex process. In the present case of planar geometry, however, this becomes an easy task for even complex channel geometries. For our studies, in which we examine vWF's shear dependent hemostatic potency, the

TABLE I. Maximum values of equivalent shear rate and velocity magnitude before and behind the bifurcation, 10 μm above the bottom wall. The results have been extracted from the lattice Boltzmann simulations.

Variable	Region	
	Before bifurcation	Behind bifurcation
Maximum shear rate	4.42/s	3.17/s
Maximum velocity	0.045 mm/s	0.032 mm/s

main coating of the track is collagen, which is known to present a vWF binding site.[36,37] The inside of the channel is coated with collagen type I (C7661, Sigma Aldrich, St. Louis, USA) in a concentration of $c \approx 10$ μg/cm^2 as previously published.[36]

2. Biofunctionalization with collagen and vWF

After the collagen coating was deposited as described above, a layer of plasmatic vWF (Baxter, Vienna, Austria) in PBS buffer solution with a concentration of $c \approx 70$ μg/μl was added. In order to achieve an effective coating, we allowed the vWF in the solution to precipitate over a few hours onto the collagen layer before beginning adhesion experiments.

To block the vWF adhesion sites, in order to show the specificity of melanoma cell-vWF adhesion, a concentrated stock solution (c=1.3 mg/ml) of purified antihuman polyclonal vWF antibody (host: rabbit) was used. For the blocking purposes, the antibody was diluted in PBS++ in a ratio of 1:20 before use and 20 μl of the antibody solution was added to the vWF coated flow chamber channel and allowed to incubate at room temperature for 20 min. After incubation, unbound antibody was removed by washing the channel with PBS++ and experiments were conducted.

E. Cells and cell culture

Melanoma cells of the amelanotic subclone A7, with maximized migration activity resulting from transfection with actin binding protein, were used for all of the experiments. Cells were cultured in a cell medium consisting of Eagle's MEM media (PAA, Leipzig, Germany) supplemented with 10% fetal calf serum (Biochrom, Berlin, Germany) and 1% penicillin/streptomycin (PAA, Leipzig, Germany). Cells were grown to confluence, removed with trypsin and resuspended in the cell medium, before being injected into the microchannels.

III. RESULTS AND DISCUSSION

It has previously been shown that freely circulating melanoma cells can firmly bind to the extracellular matrix of the blood vessel possibly initiated by integrins.[38,39] In a first step toward understanding the fundamental principles of vWF-melanoma cell interactions, we here study melanoma cell adhesion under low flow conditions (v $\sim$ 1 mm/s–5 mm/s) in different microfluidic geometries before tackling the more complex scenario of high shear flow conditions. To demonstrate the flexibility of the setup and to analyze the impact of the geometry on adhesion, we employed a design consisting of a simple (straight) channel and a channel merging into a bifurcation. Prior to the actual adhesion experiments, the flow profiles were thoroughly analyzed and characterized in a manner combining theory and experiment.

A. Hydrodynamic characterization

From the analytical solutions of the channel flow, one obtains the equivalent shear rate and velocity near the footprint of the channel, cf. Table I. The entire cross section of the equivalent shear rate at h=10 μm above the bottom wall is shown in Fig. 2(a). This distance corresponds to approximately the radius of the melanoma cells. The Reynolds number at the inlet of the channel
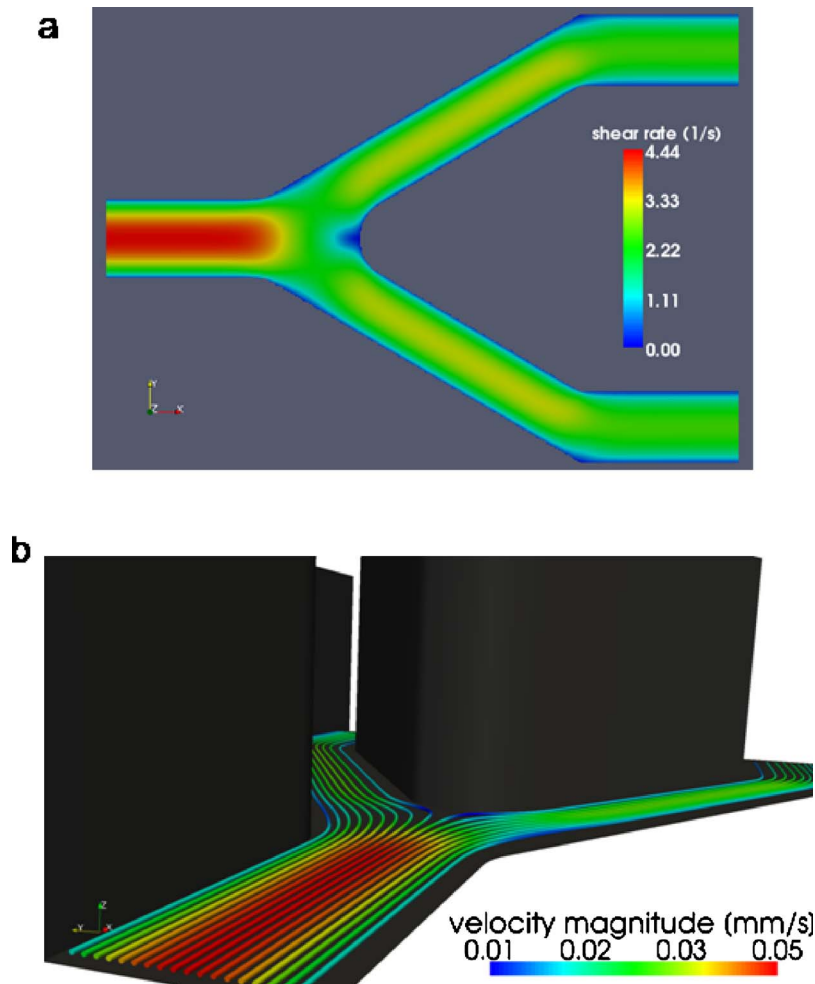
FIG. 2. (a) The simulated profile of the equivalent shear rate, 10 μm above the bottom wall of the channel. Using the experimentally extracted velocity profile, the shear rates can be quantitatively calculated and the maximum shear rate is $\dot{\gamma}=4.4/$s in front of and $\dot{\gamma}=3.2/$s behind the bifurcation. (b) Streamlines of tracer particles near the bottom wall. The initial distance to the wall is 10 μm and remains almost constant during the entire travel through the bifurcation.

is of order unity, the Reynolds number of the object of the size of a cell is smaller by a factor of approximately 100. The maximum near-bottom velocities and shear rates (10 μm above the bottom wall) are v=0.045 mm/s and $\dot{\gamma}=4.4/$s in front of the bifurcation and v=0.032 mm/s and $\dot{\gamma}=3.2/$s behind the bifurcation, respectively, and the values in front of the bifurcation are 1.4 times larger than those afterward.

Streamlines for tracer particles near the bottom wall are shown in Fig. 2(b). The simulations show that particles initially moving in x-direction remain roughly at the same distance of the bottom wall. This is because the vertical component of the velocity is very small as compared with those components parallel to the bottom wall. As a consequence, particles near the center of the channel inlet will never come close to the bottom. However, this is only true for dilute suspensions, where the overall velocity profile is not significantly influenced by the presence of the particles. In the present study, this is well justified and important as it ensures that only a small number of cells will be able to collide and bind to the surface. It points out that the laminarity of the flow conditions in such channels will keep 95% of the cells off the wall. This must be taken into consideration when calculating binding constants or substrate affinity. Numbers assuming a simple bulk/surface equilibrium, i.e., taking all immersed cells into account, will be off by up to a factor of 100, indicating a major underestimation of binding constants.
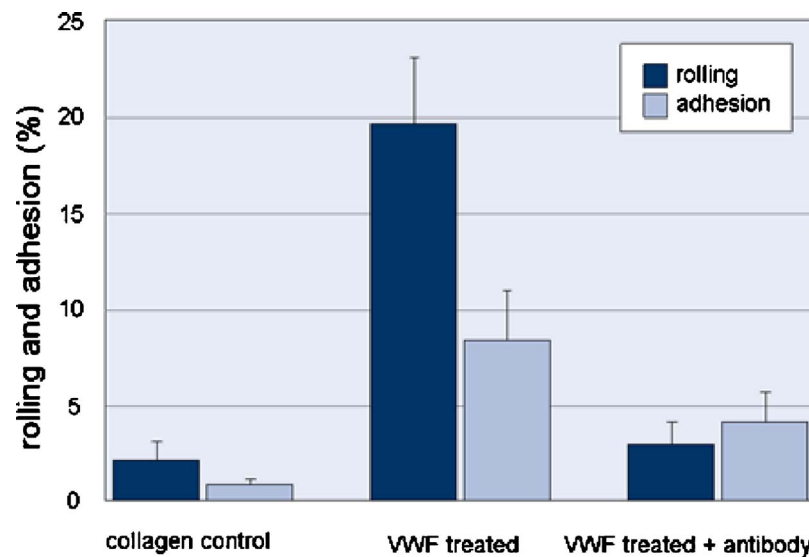
FIG. 3. Melanoma cell rolling and adhesion to collagen and vWF. Rolling and adhesion to collagen coated surface (control), vWF treated surface, and vWF surface blocked with vWF antibody. The results show a strong increase in rolling and adhesion to vWF treated surface which is entirely blocked through addition of a vWF-antibody.

B. Biofunctionalized μ-channels

In order to mimic a damaged vessel wall or an activated endothelium (followed by vWF release), we first studied the adhesion of melanoma cells on collagen without vWF coated microfluidic channels. We used collagen type I because of the well known adhesive properties, its abundance in the vessel wall, and its binding affinity to vWF as published previously.[36]

1. Straight channels

In previous publications, we have demonstrated that melanoma cells obtain an intrinsic ability to activate endothelial cells.[40] Melanoma cells derived MatrixMetalloProtease1 (MMP1) target endothelial ProteinaseActivatedReceptor1 (PAR1) followed by Weibel–Palade body exocytosis and therefore vWF release. Tumor cell induced vWF release was shown to bind and immobilize platelets at the luminal endothelial cell membrane even under high shear flow conditions.[37] We began our investigations using the most simple microvascular geometry, the straight channel in the form of an oval "track" with rounded corners. The channel surfaces were biofunctionalized with either vWF collagen or collagen alone (control) and were used to investigate the specific interaction between vWF and melanoma cells under shear stress conditions. For our studies, the flow rates were chosen to best mimic the microfluidic conditions found in the areas of our vascular system where melanoma-vWF interaction would seem most likely.

The results of our experiments are shown in Fig. 3. The average maximum cellular flow velocity for all experiments was $v=716$ μm/s with a standard deviation of SD=147 μm/s. All cells immobilized to the surface for more than 5 s were considered as adhered; however, there was no incidence of an adhered cell that became detached and remobilized during the 30 s video segments examined. Rolling cells were easily identifiable due to the characteristic "tumbling" pattern they exhibited. A rolling cell that went on to adhere was only counted once, as adhering cell. A significant increase in both rolling behavior and adhesion of melanoma cells to stretched vWF in comparison to collagen treated controls is evident. Rolling dramatically increased from $\sim$2% (SD$\pm$1.07%, n=5) for the collagen-only coated surface by a factor of 10 to $\sim$20% (SD$\pm$3.52%, n=5) for the vWF coating. Similar, melanoma cell adhesion exhibits an increase by a factor of 8 from $\sim$1% (SD$\pm$0.36%, n=5) to $\sim$8% (SD$\pm$2.67%, n=5). Here only cells in
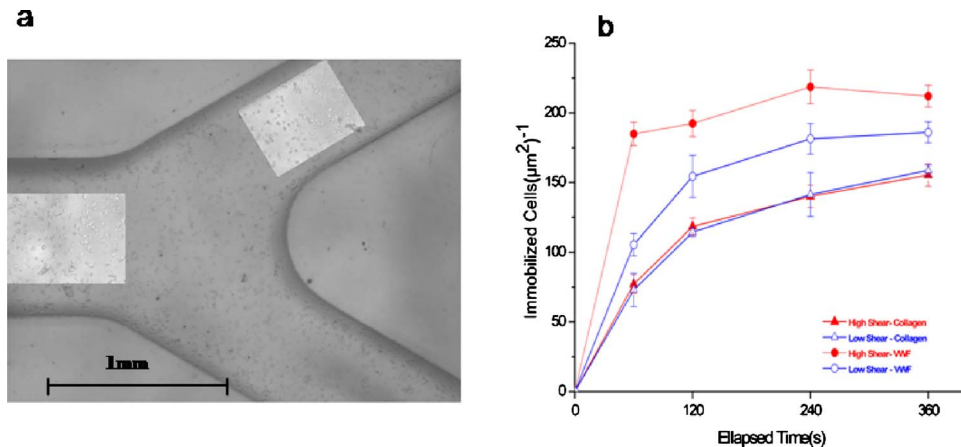
FIG. 4. (a) A schematic representation of living melanoma cells under flow inside a biofunctionalized μ-channel. The bifurcation region is captured through a 2.5× objective. A zoom-in view (highlighted boxes) of the regions before and after bifurcation is shown and indicates where measurements have taken place. (b) Cancer cell immobilization under flow for different biofunctionalized surfaces and hydrodynamic conditions. Collagen and vWF coats have been tested. The melanoma cell adhesion on the collagen coated μ-channel (filled and open triangles) does not show shear rate dependent behavior. This is in contrast to the melanoma cell immobilization in the vWF coated channel (filled and hollow circles), where an increase in shear leads to an increase in adhesion under otherwise identical hydrodynamic condition.

a 20 μm thin layer above the channel surface were taken into account. When all cells are taken as a reference the relative amount of adhered cells was only 0.01%–0.02% indicating the significance of the results presented in Fig. 2(b).

In order to further verify that vWF is the important factor in these cell-surface interactions, we attempted to block the increased adhesion by adding polyclonal vWF antibodies. For these experiments, the surfaces were again coated with collagen and stretched vWF as described. vWF antibodies were then added under laminar flow conditions to assure a homogeneous binding of antibodies throughout the channel. Confirming our expectations, the addition of vWF antibodies did indeed block both, rolling and adhesion of melanoma cells under laminar flow conditions down to values approaching those measured for collagen alone (Fig. 3). Rolling decreased to ~3% (SD $\pm$ 2.13%, n=5) and adhesion decreased to ~4% (SD $\pm$ 2.89%, n=5).

2. Bifurcated channels

Although the last paragraph clearly demonstrated the impact of vWF on melanoma cell adhesion, a more complex flow system would be beneficial. (i) From a mechanical point of view it resembles physiological flow conditions in our microvascular system more accurately. (ii) From an experimental point of view it allows to screen for the impact of different geometries simultaneously. The channel geometry shown in Fig. 1(c) for example features both straight as well as bifurcated flow conditions. The flow velocity within the channel was measured before cells were added using d=9.6 μm (Fluorescent Yellow Green Sulfate Latex, Interfacial Dynamics Corporation, Portland, Oregon, USA) beads and the corresponding wall shear rate was calculated to be $\dot{\gamma}=4.4/s$ before and $\dot{\gamma}=3.2/s$ within the bifurcation. The number of immobilized cells at the bifurcated channel bottom was monitored over time at two different positions [Fig. 4(a)]. Adhesion in the elongated and bifurcated channel parts has been analyzed. Again two different biofunctionalizations have been tested: Collagen and vWF (coated on a thick collagen layer) and a clear increase for collagen to vWF by a factor of 2 has been found [Fig. 4(b)]. Initially, the number of immobilized cells increases until the curve begins to saturate at around $t=120$ s. The zero point of the y-axis is defined by subtracting the number of cells already aggregated at the beginning of each experiment ($t=0$ s) from the total number of aggregated cell at the end of each $\Delta t=120$ s measurement period. This provides a plot of the increase in adhered cells per area and time. The slope, indicating the rate of adhesion, is almost identical for collagen coated microchannels but

different positions [Fig. 4(b)]. Furthermore, the absolute number of adhered living cells is nearly identical in both regions, demonstrating that the underlying adhesion mechanism does not depend significantly on applied shear. The reason that cell adhesion increased by a lesser degree is due to the different solutions used, which has been PBS in Fig. 3 and media (MEM) in the bifurcated channel. The proteins and sugars bind to the surface to the microfluidic channel and reduce the total amount of free binding site significantly.

Surprisingly, the increase in adhesion due to vWF is more pronounced close to the bifurcation, which reveals the importance of hydrodynamic effects for cell adhesion. Until now, we do not have any obvious explanation, but would like to hypothesize that vWF and its shear stress activation is even more pronounced in the presence of bifurcated channels.

It is important to note that given the relatively high area to volume ratio, the total number of "free" cells inside the channel cannot be considered to be constant in closed microfluidic systems. From the average number of cells adhered to the bottom of the channel, we calculate a decrease of 22%–36% in the number of flowing cells in lower laminas of flux after 120 s. The rate of decrease is dependent on the shear rate and coating of the channel. Another important property of such a microfluidic system is its laminar character. The simulation reveals that beads of one plane show only very little exchange with the adjacent laminar layers [Fig. 2(b)], implying that only very few cells are actually candidates for collisions with the bottom of the μ-fluidic channel. This renders our data somewhat insensitive to fluctuations in the total cell concentration as a fluctuation ΔN of cells in a certain volume corresponds to layer fluctuations of only $\ell \Delta N^{2/3}$, where $\ell = \Delta l / L_0$ is the relative thickness of the layer (Δl) compared with the entire channel height L_0. A total decrease in bulk concentration by $\Delta c / c_0 = 10\%$ therefore corresponds to a decrease in layer concentration of less than 5% and remains therefore within our error bars. On the flip side, it becomes clear that calculating the binding affinity based on the ratio of free-to-bound cells becomes challenging and requires a careful hydrodynamic and thermodynamic analysis. This is due to the fundamental problem of defining the system under such conditions, and is not specific to our setup.

IV. CONCLUSION

We have shown that acoustic driven μ-fluidics represents a powerful and straightforward tool for studying the adhesion of living cells on biofunctionalized complex μ-fluidic channels. It enables us to perform otherwise quite expensive inhibition studies due to the very low material requirements. The combination of our experimental investigations and computer simulations allows for a solid characterization of the hydrodynamics of the flow field and can therefore help to differentiate between biological and hydrodynamic effects. Our initial findings demonstrate that some of the previous flow chamber experiments may have to be revised since nearly 95% of the cells in the channel will not participate in the adhesion process but are hydrodynamically "trapped" in a laminar flow layer.

From a medical perspective, we found that vWF significantly increases the rate of melanoma cell adhesion in all cases studied. However, the magnitude of adhesion depends strongly on channel geometry and varies between a factor of 2 in bifurcated up to a factor of 10 in straight microfluidic channels. These differences demonstrate the necessity of both new technologies and a sophisticated interdisciplinary approach focusing on the interplay between hydrodynamic effects and soft matter.

[1] H. Al-Mondhiry, Am. J. Hematol. **16**, 193 (1984).
[2] Z. M. Ruggeri, J. N. Orje, R. Habermann, A. B. Federici, and A. J. Reininger, Blood **108**, 1903 (2006).

[3] A. Lazo-Langner, G. D. Goss, J. N. Spaans, and M. A. Rodger, J. Thromb. Haemostasis **5**, 729 (2007).

[4] C. P. W. Klerk, S. M. Smorenburg, H.-M. Otten, A. W. A. Lensing, M. H. Prins, F. Piovella, P. Prandoni, M. M. E. M. Bos, D. J. Richel, G. van Tienhoven, and H. R. Büller, J. Clin. Oncol. **23**, 2130 (2005).

[5] P. Prandoni, A. Falanga, and A. Piccioli, Lancet Oncol. **6**, 401 (2005).

[6] Z. M. Ruggeri and T. S. Zimmerman, Blood **71**, 830 (1988).

[7] K. Hoffmeister, T. Felbinger, H. Falet, C. Denis, W. Bergmeier, T. Mayadas, U. von Andrian, D. Wagner, T. Stossel, and J. Hartwig, Cell **112**, 87 (2003).

[8] S. W. Schneider, S. Nuschele, A. Wixforth, C. Gorzelanny, A. Alexander-Katz, R. R. Netz, and M. F. Schneider, Proc. Natl. Acad. Sci. U.S.A. **104**, 7899 (2007).

[9] A. Alexander-Katz, M. F. Schneider, S. W. Schneider, A. Wixforth, and R. R. Netz, Phys. Rev. Lett. **97**, 138101 (2006).

[10] N. Lion, T. C. Rohner, L. Dayon, I. L. Arnaud, E. Damoc, N. Youhnovski, W. Zhi-Yong, C. Roussel, J. Josserand, H. Jensen, J. S. Rossier, M. Przybylski, and H. H. Girault, Electrophoresis **24**, 3533 (2003).

[11] E. M. Purcell, Am. J. Phys. **45**, 3 (1977).

[12] A. van den Berg, *Lab-on-Chips for Cellomics, Micro and Nanotechnologies for Life Science* (Springer, New York, 2005).

[13] A. Wixforth, C. Strobl, C. Gauer, A. Toegl, J. Scriba, and Z. Guttenberg, Anal. Bioanal. Chem. **379**, 982 (2004).

[14] Z. Guttenberg, H. Muller, H. Habermuller, A. Geisbauer, J. Pipper, J. Felbel, M. Kielpinski, J. Scriba, and A. Wixforth, Lab Chip **5**, 308 (2005).

[15] Z. Guttenberg, A. Rathgeber, S. Keller, J. O. Radler, A. Wixforth, M. Kostur, M. Schindler, and P. Talkner, Phys. Rev. E **70**, 056311 (2004).

[16] K. Sritharan, C. J. Strobl, M. F. Schneider, A. Wixforth, and Z. Guttenberg, Appl. Phys. Lett. **88**, 054102 (2006).

[17] W. Nyborg, *Acoustic Streaming* (Academic, New York, 1965).

[18] M. F. Schneider, Z. Guttenberg, S. W. Schneider, K. Sritharan, V. M. Myles, U. Pamukci, and A. Wixforth, ChemPhysChem **9**, 641 (2008).

[19] A. Wixforth, J. Assoc. Lab. Autom. **11**, 399 (2006).

[20] L. Y. Yeo and J. R. Friend, Biomicrofluidics **3**, 012002 (2009).

[21] P. Brunet, M. Baudoin, O. Bou Matar, and F. Zoueshtiagh, Droplets Displacement and Oscillations Induced by Ultrasonic Surface Acoustic Waves: A Quantitative Study, 3 November 2009.

[22] S. Girardo, M. Cecchini, F. Beltram, R. Cingolani, and D. Pisignano, Lab Chip **8**, 1557 (2008).

[23] M. Cecchini, S. Girardo, D. Pisignano, R. Cingolani, and F. Beltram, Appl. Phys. Lett. **92**, 104103 (2008).

[24] T. Krüger, M. A. Fallah, F. Varnik, M. F. Schneider, D. Raabe, and A. Wixforth, "Inertia effects and stress accumulation in a constricted duct: A combined experimental and lattice Boltzmann study," 2010 (submitted).

[25] D. Haydock and J. Yeomans, J. Phys. A **36**, 5683 (2003).

[26] D. Haydock and J. Yeomans, J. Phys. A **34**, 5201 (2001).

[27] Y. H. Qian, D. D'Humières, and P. Lallemand, Europhys. Lett. **17**, 479 (1992).

[28] S. Succi, *The Lattice Boltzmann Equation for Fluid Dynamics and Beyond* (Oxford University Press, New York, 2001).

[29] A. J. C. Ladd and R. Verberg, J. Stat. Phys. **104**, 1191 (2001).

[30] B. Dünweg and A. J. C. Ladd, *Lattice Boltzmann Simulations of Soft Matter Systems*, Advanced Computer Simulation Approaches for Soft Matter Sciences III, Advances in Polymer Science Vol. 221 (Springer, New York, 2009), p. 89.

[31] M. Krafczyk, M. Cerrolaza, M. Schulz, and E. Rank, J. Biomech. **31**, 453 (1998).

[32] A. M. Artoli, A. G. Hoekstra, and P. M. A. Sloot, J. Biomech. **39**, 873 (2006).

[33] D. Leitner, S. Wassertheurer, M. Hessinger, and A. Holzinger, Elektrotechnik und Informationstechnik **123**, 152 (2006).

[34] D. Wang and J. Bernsdorf, *Computers and Mathematics with Applications* Vol. 58, pp. 1024–1029, 2009.

[35] PARAVIEW, June 2009, http://www.paraview.org/.

[36] A. Barg, R. Ossig, T. Goerge, M. F. Schneider, H. Schillers, H. Oberleithner, and S. W. Schneider, "Soluble plasma-derived von Willebrand factor assembles to a hemostatically active filamentous network," Thromb. Haemostasis **97**, 514 (2007).

[37] T. Goerge, F. Kleineruschkamp, A. Barg, E. M. Schnaeker, V. Huck, M. F. Schneider, M. Steinhoff, and S. W. Schneider, Thromb. Haemostasis **98**, 283 (2007).

[38] D. G. Menter, L. Fitzgerald, J. T. Patton, L. V. McIntire, and G. L. Nicolson, Immunol. Cell Biol. **73**, 575 (1995).

[39] J. Pilch, R. Habermann, and B. Felding-Habermann, J. Biol. Chem. **277**, 21930 (2002).

[40] T. Goerge, A. Barg, E.-M. Schnaeker, B. Poppelmann, V. Shpacovitch, A. Rattenholl, C. Maaser, T. A. Luger, M. Steinhoff, and S. W. Schneider, Cancer Res. **66**, 7766 (2006).